

Short communication

Isotope effect in formaldehyde steam reforming on Pt/m-ZrO₂: Insight into chemical promotion by alkalis

Michela Martinelli^a, Jonas Marcelle^b, Donald C. Cronauer^c, A. Jeremy Kropf^c, Gary Jacobs^{b,d,*}

^a Center for Applied Energy Research, University of Kentucky, 2540 Research Park Dr., Lexington, KY 40511, USA

^b University of Texas at San Antonio, Department of Biomedical Engineering and Chemical Engineering, 1 UTSA Circle, San Antonio, TX 78249, USA

^c Argonne National Laboratory, Lemont, IL 60439, USA

^d University of Texas at San Antonio, Department of Mechanical Engineering, 1 UTSA Circle, San Antonio, TX 78249, USA



ARTICLE INFO

Keywords:

Platinum / zirconia

Sodium

Alkali

Formaldehyde steam reforming

Hydrogen production

Isotope effect

ABSTRACT

Infrared spectroscopy, temperature programmed reaction mass spectrometry (TP-reaction/MS), and catalyst testing were used to investigate alkali promotion of dehydrogenation selectivity during formaldehyde steam reforming (FSR) on Pt/m-ZrO₂. In a preferred pathway, formaldehyde reacts with water forming hydrogen and formate, followed by forward formate decomposition to CO₂ and H₂. Alkali-doping of 2 wt% Pt/m-ZrO₂ increases catalyst basicity, which weakens the formate C—H bond promoting formate dehydrogenation / decarboxylation. Promotion by alkali in FSR was observed through a formate $\nu(\text{CH})$ band shift to lower wavenumbers in infrared spectroscopy, and through a decrease in the normal isotope effect in switching from H- to D-labeled formaldehyde in TP-reaction/MS.

1. Introduction

Formaldehyde steam reforming is important for a number of reasons. Light oxygenate molecules such as formic acid [1–3], formaldehyde [4–6], methanol [2,3,7], acetic acid [8], and ethanol [9–11] are being investigated as potential liquid chemical carriers of hydrogen for use in fuel cell applications. Formaldehyde steam reforming (FSR) is also a potential abatement method [12], considering that formaldehyde is toxic and volatile, and it is abundantly used in industry for producing resins and coatings, as a tissue preservative, and as a biocide. In addition, formaldehyde and acetaldehyde are potentially intermediates in the catalytic steam reforming of methanol [2,13,14] and ethanol [15,16], respectively, and therefore, shedding light on the reaction mechanism is important. Due to its higher hydrogen content, methanol has the potential to release more H₂ compared to formic acid and formaldehyde. Only a few studies are available in the literature regarding the performance [4,6,17–19] and mechanism [20,21] of supported metal FSR catalysts. Recently, we examined a series of Na-doped 2 wt% Pt/m-ZrO₂ catalysts for FSR and results of infrared spectroscopy of temperature-stepped FSR suggested that adding Na at a level of 1.8 to 2.54% Na facilitated C—H bond weakening of formate intermediate [5]. This was found to promote the dehydrogenation /

decarboxylation pathway. This Na-doping level was also found to promote forward formate decomposition in steam gas stream to H₂ and CO₂ [22], as well as the dehydrogenation / decarboxylation pathway during formic acid and methanol steam reforming [3], and the demethanation / decarboxylation in ethanol steam reforming (ESR) [23]. Alkali levels of 0.75% Li [24,25], 2.55% K [26,27], 4.65% Rb [27,28], and 5.78% Cs [29,30] were also observed to promote forward formate decomposition in steam and increase the acetate demethanation / decarboxylation pathway in ESR.

In the current investigation, the mechanism of FSR was probed by using both in-situ DRIFTS and temperature programmed FSR with mass spectrometry over unpromoted 2 wt% Pt/m-ZrO₂ and the same catalyst promoted by 0.75% Li, 1.8 and 2.54% Na, 2.55% K, 4.65% Rb, and 5.78% Cs. Moreover, temperature programmed FSR with mass spectrometry was used to compare isotope effects over unpromoted 2%Pt/m-ZrO₂ and 2.54%Na-2%Pt/m-ZrO₂ and shed further light on the role played by the alkali promoter during FSR.

* Corresponding author at: University of Texas at San Antonio, Department of Biomedical Engineering and Chemical Engineering, 1 UTSA Circle, San Antonio, TX 78249, USA.

E-mail address: gary.jacobs@utsa.edu (G. Jacobs).

<https://doi.org/10.1016/j.catcom.2023.106668>

Received 2 February 2023; Received in revised form 11 April 2023; Accepted 13 April 2023

Available online 14 April 2023

1566-7367/© 2023 The Authors. Published by Elsevier B.V. This is an open access article under the CC BY-NC-ND license (<http://creativecommons.org/licenses/by-nc-nd/4.0/>).

2. Experimental

2.1. Preparation of catalysts

The preparation of catalysts is detailed in recent publications [22–30]. The support used in this work was m-ZrO₂ (Alfa Aesar), the platinum precursor was tetraamine platinum (II) nitrate (Alfa Aesar), and the alkalis precursors were nitrates (Alfa Aesar).

2.2. Prior characterization of catalysts

Experimental methods for BET surface area and porosity, temperature programmed reduction, temperature programmed reduction (TPR) with mass spectrometry, TPR with extended x-ray absorption fine structure (TPR-EXAFS), TPR with X-ray absorption near edge spectroscopy (TPR-XANES), EXAFS fittings, Pt L3 minus L2 edge XANES difference procedure, and in-situ DRIFTS of FSR are described in recent publications [17–25]. A detailed summary of prior characterization is provided in Table S1 (see Supplementary Information).

2.3. Temperature programmed FSR reaction with mass spectrometry

Catalysts were activated by (1) flowing 30 cm³/min of 33 vol% H₂ (balance argon) at 300 °C, (2) cooling to 225 °C and steaming for 15 min using 30 cm³/min of He gas flowed through a H₂O saturator, (3) flowing 30 cm³/min of 33 vol% H₂ (balance argon) at 225 °C for 10 min, and (4) purging in 50 cm³/min of Ar for 15 min and cooling to 50 °C in Ar gas flow. This procedure was performed to ensure that defect-associated bridging OH groups were formed on the surface of the catalyst, which is more representative of the catalyst surface during steam reforming catalysis at a high H₂O/CH₂O gas ratio. The catalyst surface was saturated by injecting 100 μl of 10 vol% formaldehyde / 90 vol% H₂O or 20 vol% D-formaldehyde / 80 vol% D₂O and then purging in 50 cm³/min of Ar to remove weakly bound adsorbed species. The catalyst was then heated at 10 °C/min to 700 °C, and the MS signals of H₂ (D₂), CO, and CO₂ were followed in order to investigate chemical steps involved in converting formaldehyde by steam.

To explore the isotope effect involved in the dehydrogenation of formate, the unpromoted 2%Pt/m-ZrO₂ and 2.54%Na-2%Pt/m-ZrO₂ catalysts were used. Two separate runs were used such that 5.4 mol% H-formaldehyde or D-formaldehyde was used with a balance of ~47.3 mol % H₂O and ~ 47.3 mol% D₂O. In this way, isotope effects relevant to reactions of C-H/C-D bonds could be investigated. The catalysts were activated in a similar manner and the MS signal of H₂ (or D₂) was followed.

2.4. Catalytic testing

The activity and selectivity performance of the catalysts was tested using a fixed bed microreactor. Briefly, 80 mg of catalyst (63–106 μm) was diluted with 300 mg of SiO₂ beads and activated using 100 cm³/min H₂ at 350 °C for 1 h. Next, the catalyst was cooled to 300 °C in Ar, and the gas was changed to a mixture containing 37.9% H₂O, 6.6% CH₂O (balance N₂) at P = 1 atm. The products were analyzed by SRI 8610 GC. The CH₂O conversion and CO_x selectivity (CO or CO₂) were calculated by using Eq. (1) and Eq. (2), respectively:

$$X_{CH_2O} = 1 - \frac{F_{CH_2O}^{out}}{F_{CH_2O}^{in}} \quad (1)$$

$$s_{CO_x} = \frac{F_{CO_x}^{out}}{(F_{CH_2O}^{in} - F_{CH_2O}^{out})} \quad (2)$$

3. Results and discussion

Table S1 compiles prior characterization of the catalysts [22–30]. A brief summary is provided. In these works, the alkali loading was varied for each Group 1 alkali promoter. As discussed previously, the catalysts were previously tested for reactions such as water-gas shift and ethanol steam reforming. The selected alkali loading for the current work is the minimum loading from each series tested, where a significant shift in the formate ν(CH) band from CO adsorption to the H₂-activated catalyst was observed while, at the same time, a high fraction of Pt⁰ active sites remained unblocked by the alkali. Similar shifts to lower wavenumbers were observed at higher loadings of alkali; however, in those cases, the Pt⁰ active sites were significantly covered. The fraction of Pt⁰ sites was monitored by examining the Pt carbonyl band region in infrared spectroscopy. These specific loadings yielded higher forward formate decomposition rates in the presence of steam to H₂ and adsorbed CO₂, and improved acetate demethanation / decarboxylation selectivities in ESR. As shown in Table S1, there is a systematic shift in the main formate ν(CH) band to lower wavenumbers with increasing alkali basicity (higher atomic number). Prior work suggested that the formate ν(CH) band shift was due to enhanced catalyst basicity. In general, temperature programmed desorption of CO₂, an acidic molecule, was less facile by the addition of the alkali promoter relative to the unpromoted catalyst, resulting in a shift in the desorption peaks to higher temperatures (Table S1). As such, the -OOC functional group in formate is expected to be held more tightly to the catalyst surface, which should weaken the formate C–H bond.

For Rh/ceria catalysts, a related system, Shido and Iwasawa [31] suggested through an investigation of the kinetic isotope effect that the rate-limiting step of formate decomposition in steam was the C–H scission of bidentate formate. The optimized Li, Na, and K-promoted Pt/m-ZrO₂ catalysts used in this work, which exhibited shifts to lower wavenumbers of the formate ν(CH) band [22,24,26] relative to the unpromoted catalyst, as shown in Table S1, had higher formate decomposition rates and higher water-gas shift reaction rates relative to the unpromoted catalysts. This suggests that despite having higher catalyst basicity, CO₂ (an acidic molecule) was not prevented from evolving in the catalytic cycle. The alkali loadings were high enough to facilitate formate dehydrogenation, but at the same time sufficient Pt⁰ remained available to facilitate both formate dehydrogenation and CO₂ removal at the metal-support interface. Higher Li, Na, and K loadings inhibited formate decomposition and CO₂ removal by blocking Pt⁰ sites and water-gas shift reaction rates diminished [22,24,26]. Higher basicity alkalis such as Rb and Cs facilitated formate dehydrogenation, but inhibited CO₂ product desorption due to enhanced carbonate stability [28,29]. For Rb and Cs catalysts, the rate-limiting step of the cycle was not the forward formate decomposition, but rather that of carbonate decomposition, and no loading of Rb or Cs was found to enhance water-gas shift reaction rates [28,29].

No evidence was found to suggest that the alkali promoter enhanced the electron density on metallic Pt clusters following activation. In contrast, for every alkali-doped catalyst examined, difference spectra from the Pt L₃ edge minus the Pt L₂ edge (i.e., isolating the valance band) revealed a higher intensity. These results [23,24,27–29] are summarized in Table S1.

Adding alkali at these weight percentages resulted in decreased surface areas (by 22–30%), and these percentage decreases are higher than what is expected assuming that the promoters add weight but not surface [23–30]. Thus, for each catalyst, a fraction of the pores is blocked by the alkali promoter. The average metal nanoparticle diameter measured by EXAFS spectroscopy was about 1 nm for all samples, except for the potassium-promoter one, where a larger size of 2.7 nm was found. Contact between alkali and platinum was strongly suggested by the fact that reduction of Pt oxide was hindered. In TPR-XANES, the temperature to achieve 50, 25, and 10% of the original white line intensity shifted to higher temperatures. Fig. S1 provides TPR-XANES and

TPR-EXAFS results near the Pt L₂ edge for the 2.55% K-2% Pt/m-ZrO₂ catalyst, while results for all the other catalysts (either at the Pt L₂ or Pt L₃ – or both) can be found in prior work.

Figs. 1 and 2 provide results of DRIFTS of FSR reaction of the unpromoted 2%Pt/m-ZrO₂ catalyst and a representative alkali-promoted catalyst, ca. 2.55%K promoted catalyst. DRIFTS of FSR reaction for the remaining alkali-promoted catalysts are found in Figs. S2 through S6 (Supplementary Information), including 0.75% Li, 1.8% Na, 2.54% Na, 4.65% Rb, and 5.78% Cs, respectively. Also, Table 1 provides a summary of the key findings from temperature stepped DRIFTS of FSR reaction. At 50 °C, the predominant surface species is already formate, likely resulting from the reaction of adsorbed formaldehyde and water, which liberated one H₂ molecule and produced surface formate. As shown in Scheme 1, formate formation may involve a concerted mechanism, or a sequence not unlike that of an associative water-gas shift reaction mechanism, where adsorbed CO-s and adsorbed H-s are formed prior to the liberation of H₂(g) and the reaction of CO with bridging OH groups (i.e., activated H₂O adsorbed at O-vacancy defects) producing formate. Surface formate species are characterized by $\nu(\text{CH})$, $\delta(\text{CH}) + \nu_{\text{sym}}(\text{OCO})$, $2\delta(\text{CH})$, $\nu_{\text{asym}}(\text{OCO})$, and $\nu_{\text{sym}}(\text{OCO})$ modes of vibration. Pt carbonyl bands were also detected in the 2100 to 1800 cm⁻¹ range. With an increase in the temperature up to 125 °C (5.78% Cs-promoted), 150 °C (unpromoted, 1.8% Na, 2.54% Na, 2.55% K, and 4.65% Rb), and 175 °C (0.75% Li-promoted), the intensities of the surface formate bands increase. Band assignments at the point of maximum formate intensity are compiled in Table 1. As previously observed with formate

species produced from CO-DRIFTS (Table S1), the main formate $\nu(\text{CH})$ band is shifted to lower wavenumbers relative to that of the unpromoted catalyst. Moreover, there is a systematic shift in the formate $\nu(\text{CH})$ band with increasing alkali basicity (atomic number). In addition to the CO₂-TPD results shown in Table S1 that suggest higher basicity, another measure of basicity comes from the difference between the $\nu(\text{OCO})$ of formate asymmetric and symmetric vibrational modes. CO₂ is an acidic molecule and a probe molecule for basicity. For the free carbonate ion, the ν_3 band is 1415 cm⁻¹ [32]. However, when CO₂ adsorbs on a metal oxide surface, it may produce carbonate species that exhibits less symmetry than the free carbonate. As such, there is a splitting of the ν_3 band on either side of 1415 cm⁻¹. In general, the greater the bonding strength, the greater the splitting between the ν_3 bands of carbonate. As such, unidentate, bidentate, and bridged carbonates (i.e., with increasing bonding strength with the surface) will show increases in $\Delta\nu_3$ splitting of ~100, 300, and 400 cm⁻¹. According to Lavalley [32], normally, unidentate will be less stable than bidentate, etc. That is, there is typically, though not always, a correlation between the $\Delta\nu_3$ splitting and resistance to thermal decomposition. An exception to the rule was reported by Busca and Lorenzelli [33], where some low $\Delta\nu_3$ splitting bands were very resistant to thermal decomposition and may correspond to polydentate structures similar to bulk species. Table 1 shows that a similar splitting of the $\nu(\text{OCO})$ asymmetric and symmetric bands occurs with the bidentate formate species ($\Delta\nu$ splitting of 200–300 cm⁻¹). With increasing basicity, the -OOC functional group is bound more tightly to the support, and this in turn weakens the -C-H bond of formate, resulting

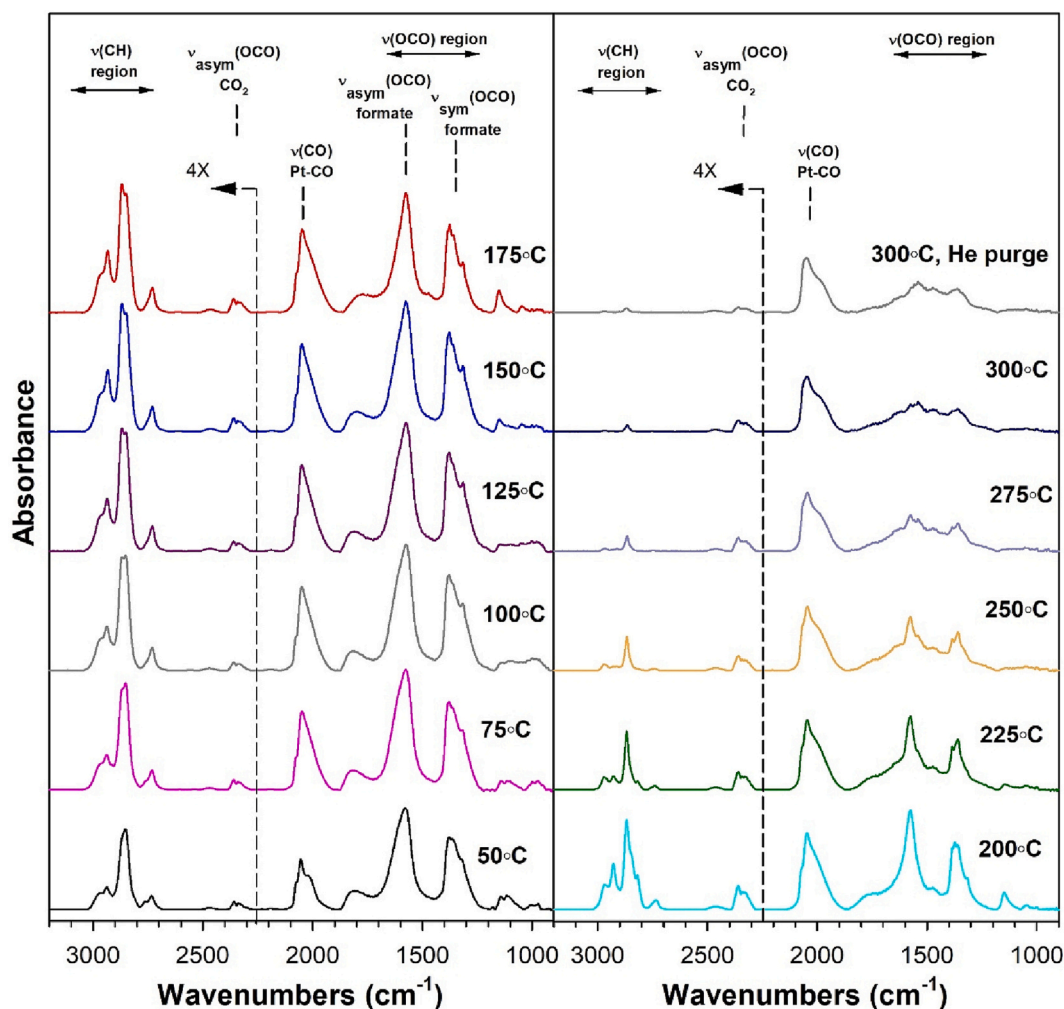


Fig. 1. DRIFT spectra of 2%Pt/m-ZrO₂, including adsorption of 10% formaldehyde in H₂O following at 50 °C He purge and then adding 4.4% H₂O at 75, 100, 125, 150, 175, 200, 225, 250, 275, and 300 °C, including a He purge for 15 min at 300 °C.

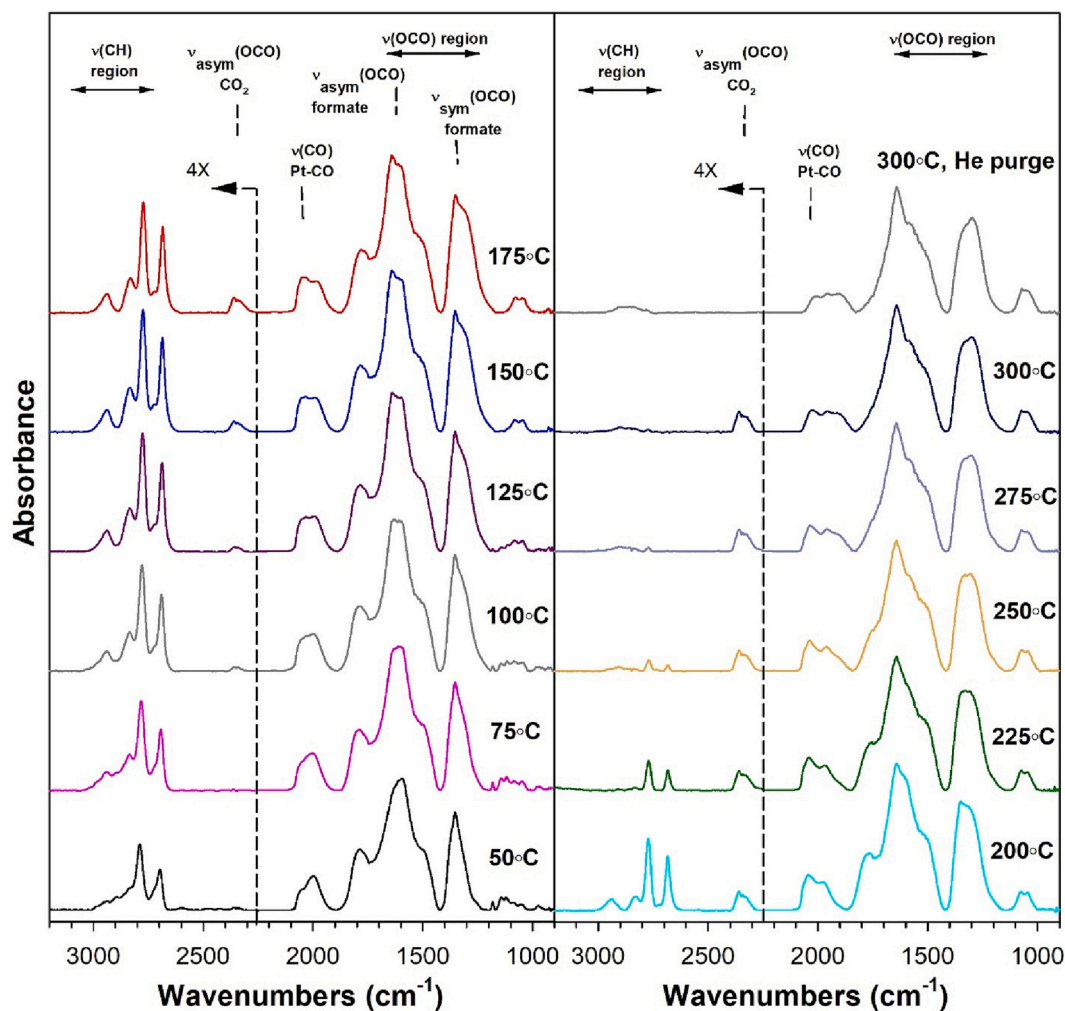


Fig. 2. DRIFT spectra of 2.55%K-2%Pt/m-ZrO₂, including adsorption of 10% formaldehyde in H₂O at 50 °C following He purge and then adding 4.4% H₂O at 75, 100, 125, 150, 175, 200, 225, 250, 275, and 300 °C, including a He purge for 15 min at 300 °C (see Supplementary Information for similar results over 0.75% Li, 1.8% Na, 2.54% Na, 2.55% K, 4.65% Rb, and 5.78% Cs promoted catalysts).

in a shift to lower wavenumbers. By moving to higher atomic number elements, the trend is increasing basicity, as cation hardness decreases (i.e., same charge, but dispersed over a greater volume). Increasing basicity is therefore proposed to increase the interaction between the -OOC functional group and the defect-laden support. As a consequence, the -C-H bond of formate is weakened. This results in a systematic decrease in the formate $\nu(\text{CH})$ band with increasing atomic number of the alkali. In prior work, we found that in order to observe the band shift, an optimum loading of the alkali was needed. That is why specific alkali loadings were used in this work.

Moving to higher temperatures, the formate species tend to react faster on the alkali-promoted catalysts such that by 225 and 250 °C, lower area-% of formate bands (as measured in the 3100–2600 cm^{-1} range relative to the maximum formate intensity) are observed (Table 1). At higher temperatures, the $\nu(\text{OCO})$ bands of residual surface carbonate species are present, indicating that surface formates underwent forward decomposition by dehydrogenation, producing CO₂. As shown in Scheme 1, increased basicity by alkali promotion facilitated the preferred formate dehydrogenation pathway, which is designated by the rate constant, k_1 .

To put these conclusions on a firmer footing, temperature programmed FSR was conducted over the series using H-formaldehyde (Fig. S7) with H₂O and D-formaldehyde with D₂O (Fig. S8). Key observations are summarized in Table 2. For the unpromoted catalyst using H-formaldehyde and H₂O (Fig. S7, subfigure a), there are two H₂ evolution

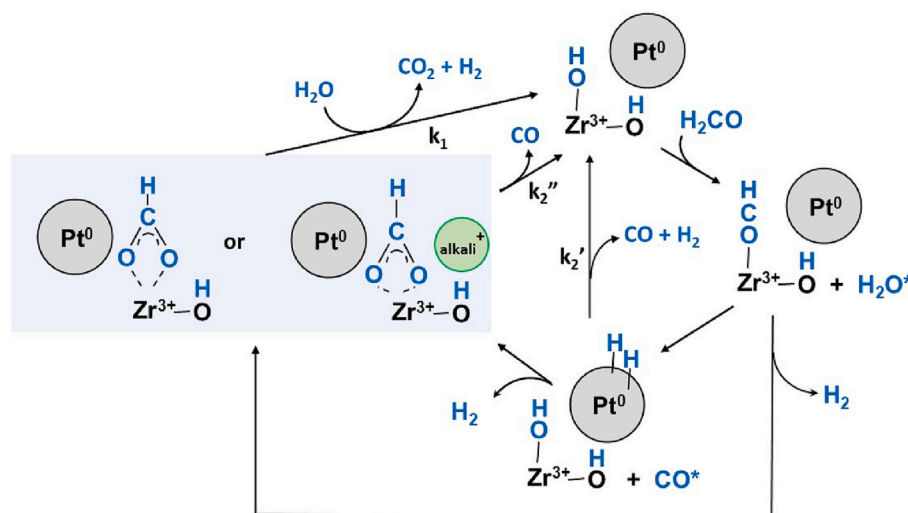
steps at ~ 154 °C and ~ 190 °C. The second step is associated with CO₂ production, which has a peak maximum at 192 °C. Thus, the first H₂ evolution step is consistent with the reaction of formaldehyde with H₂O, evolving H₂ and producing adsorbed formate, while the second step is consistent with forward formate decomposition / decarboxylation (with a rate constant, k_1). A signal for CO is also detected. Undesired decarbonylation may occur if formaldehyde dissociates to CO and hydrogen prior to the reaction of CO with bridging OH groups (i.e., activated H₂O, which is dissociated H₂O at O-vacancy defects) producing formate. In that case, the rate of decarbonylation might be high enough that some CO desorbs prior to reacting with the bridging OH groups. In Scheme 1, the rate constant for that pathway is labeled as k_2' . Another route for undesired decarbonylation is the reverse decomposition of formate to CO and adsorbed -OH, which is shown as having a rate constant k_2'' in Scheme 1. Both routes lead to an equivalent surface. Interestingly, the signal of CO evolution was highest for the unpromoted catalyst (approximately 2 to 25 times higher, depending on the identity of the alkali in the alkali-promoted catalyst). This suggests that the alkali facilitates the dehydrogenation / decarboxylation pathway, as previously discussed, increasing the $k_1/(k_2' + k_2'')$ ratio.

Adding the alkali, the first H₂ production step remains at low temperature (shoulder at 150–167 °C observed), while the maximum temperature for the second H₂ production step generally moves to lower temperatures with increasing alkali basicity. This is consistent with the role of the alkali to weaken the formate C–H bond. The CO₂ evolution

Table 1

Formate $\nu(\text{CH})$ band region at the maximum intensity and other relevant vibrational positions during temperature stepped formaldehyde/ H_2O reaction using the assignments of Binet et al. [33]. Carbonate band positions were recorded at 300 °C.

Catalyst	Formate max. intensity T (°C)	Formate $\nu(\text{CH})$	Formate $\delta(\text{CH}) + \nu_{\text{sym}}(\text{OCO})$	Formate $2\delta(\text{CH})$	Formate $\nu(\text{OCO})$ region	Carbonate $\nu(\text{OCO})$ region	$\Delta(\text{OCO})$ formate (cm^{-1})	% of Formate Band Area at 225 °C and 250 °C Relative to Maximum Area (3100–2600 cm^{-1})
2%Pt/m-ZrO ₂	150	2869, 2850	2933, (3000–2950)	2732, (2775–2745)	1576, 1386, 1378, 1363, 1316	1540, 1474, 1370, (1300–1185)	198	26.7% 12.6%
0.75%Li-2%Pt/m-ZrO ₂	175	2854, (2850–2790)	2955, (3000–2990)	2746, (2735–2692)	1628, (1417–1378), 1367, 1341, 1325	1624, (1570–1485), (1485–1445), 1354, (1315–1220)	261	26.4% 6.1%
1.8%Na-2%Pt/m-ZrO ₂	150	2842, 2803	2950, (3000–2975)	(2755–2725), 2705	1644–1606, (1372), 1362, (1352–1335), (1335–1245)	1644, (1615–1463), (1427–1330), 1316	263	3.7% 1.5%
2.54%Na-2%Pt/m-ZrO ₂	150	(2890–2830) 2803	2956, (3000–2985)	(2760–2720) 2706	1621, 1560–1472, 1358, (1345–1190)	1636, (1612–1474), 1327	263	8.8% 3.3%
2.55%K-2%Pt/m-ZrO ₂	150	2833, 2775	2937, (3000–2965)	2686, 2726	1641, (1625–1540), (1540–1440), 1352, (1340–1175)	1641, (1594–1435), (1400–1320), 1297	289	15.3% 4.3%
4.65%Rb-2%Pt/m-ZrO ₂	150	2829, 2766	2934	2679, 2722	1647, (1623–1537), (1537–1426), 1349, (1320–1187)	1645, 1569, 1331, 1274	298	21.6% 5.7%
5.78%Cs-2%Pt/m-ZrO ₂	125	2830, 2761	2932, (3000–2950)	2675, 2722	1644, 1594, (1520–1425), 1345, (1337–1305, 1305–1200)	1644, (1590–1495), (1495–1420), (1385–1325), 1267	299	11.1% 1.5%

**Scheme 1.** Formaldehyde steam reforming pathways and the role of the alkali promoter.

step moves to temperatures higher than the second H_2 production step, due to the enhanced basicity of the catalyst surface, which results in a stronger interaction with adsorbed CO_2 . Once again, decarbonylation is significantly reduced with the addition of the alkali to the catalyst. With all of the catalysts, additional broad peaks for H_2 / CO_2 evolution are observed at higher temperatures, which may be due to formate species located further from Pt nanoparticles/support interface, that require surface diffusion prior to reaction at the Pt-support interface. The decrease in decarbonylation selectivity for alkali-promoted catalysts is also observed during the catalytic testing of FSR (Table 3) as a CO_2 selectivity of 100% is observed for 0.75% Li and 2.54% Na-promoted catalysts. In contrast, the CO_2 selectivity was only 82.5% for the unpromoted catalyst.

In examining the series using D-formaldehyde and D_2O (Fig. S8), similar trends are observed as with the hydrogen labeled series. However, two additional important conclusions can be drawn. First, the D_2 evolution peaks are shifted to higher temperature due to a normal isotope effect associated with C–H / C–D bond breaking and/or O–H /

O–D bond breaking, with C–D and O–D being stronger bonds relative to C–H and O–H. Secondly, there is a connection between a faster dehydrogenation / decarboxylation pathway and forward formate decomposition. This can be observed by comparing the extent of decarbonylation when H- or D-labels are being used. When the D-label is used, forward formate decomposition by dehydrogenation / decarboxylation is significantly hindered. As such, decarbonylation selectivity increases. As shown in Table 2, the percentage of CO evolved when the H-label was used versus when the D-label was used for the unpromoted catalyst was just 35%.

In order to assess the normal isotope effect involved in C–H bond breaking of formate during the forward formate decomposition step (i. e., the second H_2 evolution step in FSR), it was necessary to control the isotopic labeling of the water. To accomplish this, equivalent 47.3% / 47.3% molar amounts of H_2O and D_2O were used in the mixture with either the H- or D-labeled formaldehyde in separate runs over each catalyst. These tests were conducted for both unpromoted 2%Pt/m-ZrO₂ and the 2.54%Na-2%Pt/m-ZrO₂ catalyst. Plots are provided in Fig. 3,

Table 2

Results of temperature programmed FSR reaction using H₂O and H-formaldehyde (top) and D₂O and D-formaldehyde (bottom).

	H ₂ Step #1 (°C)	H ₂ Step #2 (°C)	CO (°C)	CO ₂ (°C)	% CO peak < 225 °C area relative to 2% Pt/m-ZrO ₂	% CO peak < 225 °C area relative to 2% Pt/m-ZrO ₂ deuterated
2%Pt/m-ZrO ₂	154	190	159	192	100.0	35.0%
0.75%Li-2%Pt/m-ZrO ₂	(< 167)	177	164	196	42.9	15.0%
1.8%Na-2%Pt/m-ZrO ₂	(< 155)	164	156	165	36.4	12.7%
2.54%Na-2%Pt/m-ZrO ₂	(< 150)	170	156	188	4.3	1.5%
2.55%K-2%Pt/m-ZrO ₂	(< 150)	160	151	161	8.6	3.0%
4.65%Rb-2%Pt/m-ZrO ₂	(< 150)	158	151	169	22.1	7.7%
5.78%Cs-2%Pt/m-ZrO ₂	(< 150)	155	159	170	16.8	5.9%

	D ₂ Step #1 (°C)	D ₂ Step #2 (°C)	CO (°C)	CO ₂ (°C)	% CO peak < 225 °C area relative to 2%Pt/m-ZrO ₂
2%Pt/m-ZrO ₂	(< 165)	219	169	222	100.0
0.75%Li-2%Pt/m-ZrO ₂	(< 176)	210	181	238	38.1
1.8%Na-2%Pt/m-ZrO ₂	(< 175)	192	168	238	19.8
2.54%Na-2%Pt/m-ZrO ₂	(< 165)	172	163	220	4.2
2.55%K-2%Pt/m-ZrO ₂	(< 156)	169	159	178	24.4
4.65%Rb-2%Pt/m-ZrO ₂	(< 162)	171	164	192	20.7
5.78%Cs-2%Pt/m-ZrO ₂	(< 157)	165	160	179	9.9

Table 3

Selectivity for the unpromoted and alkali-promoted catalysts at similar conversion at 300 °C.

	CH ₂ O conversion (%)	CO selectivity (%)	CO ₂ selectivity (%)
2%Pt/m-ZrO ₂	86.00	17.49	82.51
2.54%Na-2%Pt/m-ZrO ₂	89.78	–	100
0.75%Li-2%Pt/m-ZrO ₂	89.68	–	100

while the isotope effect results are reported in Table 4. Here, only the second step of H₂ (or D₂) evolution is reported in Table 4 for the four profiles – H versus D for unpromoted versus 2.54%Na-promoted catalyst. First of all, the temperature of the second H₂ (or D₂) production step was lower for the 2.54%Na promoted catalyst relative to that of the unpromoted catalyst. Moreover, the difference in temperature between the second H₂ production and the second D₂ production steps (i.e., associated with formate dehydrogenation) is smaller for the 2.54%Na promoted catalyst relative to that of the unpromoted catalyst. Both findings are consistent with a role of the alkali promoter being to weaken the C–H bond of formate during FSR reaction. A rough estimate can be made by applying the Redhead method to TP-reaction, where the

activation energy is correlated with T_{max} for the reaction step of interest and the pre-exponential factor is assumed to be identical for H- versus D-labeled cases. With this estimate, the normal isotope effect decreases from ~2.4 for the unpromoted catalyst to ~1.6 for the 2.54%Na-promoted catalyst.

Pinpointing isotope effects provides valuable information about the breaking or formation of a chemical bond at either the rate determining step or product formation steps. In the current context, the difference in the magnitudes of the isotope effect involved in the second hydrogen formation step of FSR was determined for unpromoted and 2.54%Na-promoted catalysts. The decrease in the magnitude of the isotope effect, coupled with important changes in selectivity (i.e., favoring decarboxylation of the intermediate relative to decarbonylation), provided insights into the nature of the chemical promotion by Na. Furthermore, over a series of alkali-promoted catalysts, using deuterium-labeled formaldehyde with D₂O in lieu of the H-labeled molecules allowed a slowing of the temperature programmed surface reaction so that the temperature maxima of different steps involved in the turnover of adsorbed formaldehyde and subsequent intermediates could be better resolved.

4. Conclusions

By comparing the results from in-situ DRIFTS of FSR reaction with those from temperature programmed FSR reaction and utilizing H- and D-labeled feed mixtures, a number of conclusions can be drawn. DRIFTS results indicated that significant formate is already formed even at 50 °C. With increasing temperature up to ~150 °C +/- 25 °C, formate increased in intensity in DRIFTS. In TR-FSR, there was hydrogen liberation without significant CO₂ liberation. Thus, the first H₂ production step is likely the reaction of H₂O with adsorbed formaldehyde to produce formate and H₂.

Above this temperature, formate decomposes by dehydrogenation / decarboxylation. CO₂ and H₂ were evolved concurrently for the unpromoted catalyst, while for the alkali-promoted catalysts, the basicity is higher, thus CO₂ was retained to higher temperatures than the H₂ evolution. Adding the alkali at optimized levels weakens the formate C–H bond. As such, this second H₂ evolution step occurred at significantly lower temperatures for the alkali-promoted catalysts. Moreover, there is less decarbonylation by adding alkali promoter, because the rate of the decarboxylation/dehydrogenation pathway is enhanced. For the case of D-formaldehyde reacting with D₂O, the C–D bond of D-formate is stronger than that of C–H of H-formate (when H-formaldehyde is reacted with H₂O), so with the D-label the dehydrogenation/decarboxylation pathway is kinetically restricted, resulting in a higher rate of decarbonylation for D- relative to the H-label.

In running the isotope effect in TP-FSR for the unpromoted and 2.54% Na promoted catalysts using equivalent amounts of H- and D-labeled steam (47.3% H₂O / 47.3% D₂O, molar basis) with either H-formaldehyde or D-formaldehyde, there was a normal isotope effect. The normal isotope effect is greater for the unpromoted catalyst (~2.4) in comparison to that of the Na-doped catalyst (~1.6), due to the involvement of the Na promoter in weakening the C–H (C–D) bond of formate. This is a direct result of the higher basicity of the alkali-promoted catalyst, where the -OOC functional group of formate is held more tightly to the catalyst surface, thereby weakening the formate C–H bond. This enhanced basicity for the alkali-promoted catalysts was observed by the greater $\nu(\text{OCO})$ splitting of the asymmetric and symmetric bands in formate, as well as the greater thermal stability of adsorbed CO₂ in the CO₂-TPD experiments.

CRedit authorship contribution statement

Michela Martinelli: Formal analysis, Investigation, Visualization, Validation, Writing – original draft, Writing – review & editing. **Jonas Marcelle:** Formal analysis, Investigation, Validation. **Donald C.**

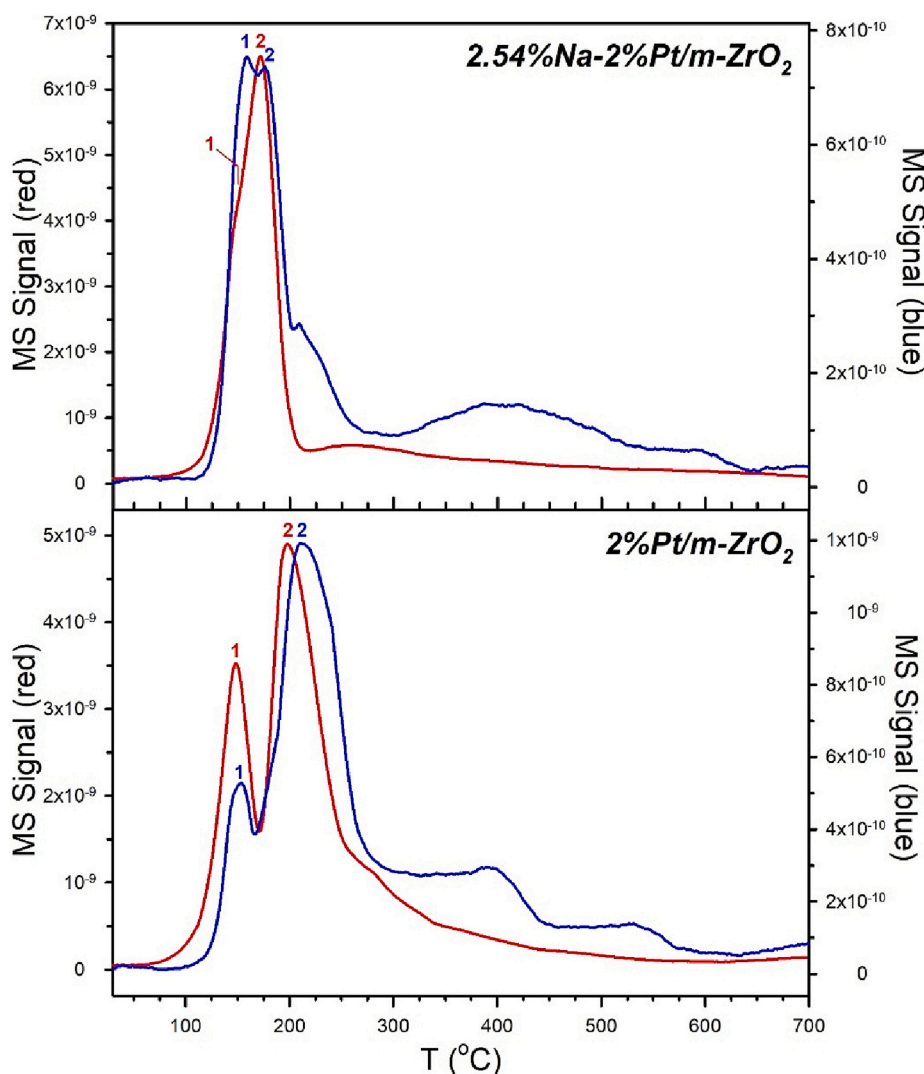


Fig. 3. TP-reaction of adsorbed mixture of (red) 5.4 mol% H-formaldehyde / 47.3 mol% H₂O / 47.3 mol% D₂O or (blue) 5.4 mol% D-formaldehyde / 47.3 mol% H₂O / 47.3 mol% D₂O over (bottom) 2%Pt/m-ZrO₂ and (top) 2.54%Na-2%Pt/m-ZrO₂. (red) H₂ and (blue) D₂. (For interpretation of the references to colour in this figure legend, the reader is referred to the web version of this article.)

Table 4

Isotope effect in Step #2 from Redhead analysis of temperature programmed reaction using equivalent moles of H- or D-labeled formaldehyde and a 47.3% / 47.3% mixture of H₂O / D₂O.

	H or D	T _{max} (°C)	E _{act} (kJ/mol)	ΔE _{act} (kJ/mol)	NIE	(NIE with Na) / (NIE without Na)
2%Pt/m-ZrO ₂	H	199	134.4	2.9	2.4	0.67
	D	209	137.3			
2.54%Na-2%Pt/m-ZrO ₂	H	171	126.2	1.5	1.6	0.67
	D	176	127.7			

Cronauer: Supervision, Investigation, Resources. **A. Jeremy Kropf:** Data curation, Investigation, Resources, Supervision. **Gary Jacobs:** Conceptualization, Formal analysis, Investigation, Supervision, Visualization, Validation, Writing – original draft, Writing – review & editing, Project administration.

Declaration of Competing Interest

The authors declare that they have no known competing financial

interests or personal relationships that could have appeared to influence the work reported in this paper.

Data availability

The authors do not have permission to share data.

Acknowledgments

The work of Gary Jacobs and Jonas Marcelle was funded in part by a UTSA-SWRI Connect grant supported by The Office of the Vice President for Research, Economic Development, and Knowledge Enterprise at UTSA. Argonne's research was supported in part by the U.S. Department of Energy (DOE), Office of Fossil Energy, National Energy Technology Laboratory (NETL). The Advanced Photon Source was supported by the U.S. Department of Energy, Office of Science, Office of Basic Energy Sciences, under contract number DEAC02-06CH11357. MRCAT operations are supported by the Department of Energy and the MRCAT member institutions. CAER research was supported by the Commonwealth of Kentucky.

Appendix A. Supplementary data

Supplementary data to this article can be found online at <https://doi.org/10.1016/j.catcom.2023.106668>.

References

- [1] J. Li, P. Jia, X. Hu, D. Dong, G. Gao, D. Geng, J. Xiang, Y. Wang, S. Hu, Steam reforming of carboxylic acids for hydrogen generation: effects of aliphatic chain of the acids on their reaction behaviors, *Molec. Catal.* 450 (2018) 1–13, <https://doi.org/10.1016/j.mcat.2018.02.027>.
- [2] G. Jacobs, P.M. Patterson, U.M. Graham, A.C. Crawford, A. Dozier, B.H. Davis, Catalytic links among the water–gas shift, water-assisted formic acid decomposition, and methanol steam reforming reactions over Pt-promoted thoria, *J. Catal.* 235 (2005) 79–91, <https://doi.org/10.1016/j.jcat.2005.07.010>.
- [3] M. Martinelli, G. Jacobs, W.D. Shafer, B.H. Davis, Effect of alkali on C–H bond scission over Pt/YSZ catalyst during water-gas-shift, steam-assisted formic acid decomposition and methanol steam reforming, *Catal. Today* 291 (2017) 29–35, <https://doi.org/10.1016/j.cattod.2016.12.003>.
- [4] L. Chu, Y. Shen, Hydrogen production from formaldehyde steam reforming using recyclable NiO/NaCl catalyst, *Appl. Surf. Sci.* 532 (2020) 147376, 10, <https://doi.org/10.1016/j.apsusc.2020.147376>.
- [5] M. Martinelli, E.S. Garcia, C.D. Watson, A.J. Kropf, D.C. Cronauer, G. Jacobs, Na promotion of Pt/m-ZrO₂ catalysts for the steam reforming of formaldehyde, *Catalysts* 12 (2022) 1294, 19, <https://doi.org/10.3390/cata11211294>.
- [6] L. Chu, S. Gu, Q. Jin, P. Zhu, Y. Shen, P. Li, Hydrogen production from formaldehyde steam reforming using recyclable NiO/NaF catalyst, *Internat. J. Hyd. Energ.* 45 (2020) 28752–28763, <https://doi.org/10.1016/j.ijhydene.2020.07.223>.
- [7] L. Lin, W. Zhou, R. Gao, S. Yao, X. Zhang, W. Xu, S. Zheng, Z. Jiang, Q. Yu, Y.-W. Li, C. Shi, X.-D. Wen, D. Ma, Low-temperature hydrogen production from water and methanol using Pt/α-MoC catalysts, *Nature* 544 (2017) 80–83, <https://doi.org/10.1038/nature21672>.
- [8] L. Zhang, X. Hu, K. Hu, Hu Cathy, Z. Zhang, Q. Liu, S. Hu, J. Xiang, Y. Wang, S. Zhang, Progress in the reforming of bio-oil derived carboxylic acids for hydrogen generation, *J. Power Sources* 403 (2018) 137–156, <https://doi.org/10.1016/j.jpowsour.2018.09.097>.
- [9] D.K. Liguras, D.I. Kondarides, X.E. Verykios, Production of hydrogen for fuel cells by steam reforming of ethanol over supported noble metal catalysts, *Appl. Catal. B Environ.* 43 (2003) 345–354, [https://doi.org/10.1016/S0926-3373\(02\)00327-2](https://doi.org/10.1016/S0926-3373(02)00327-2).
- [10] L.V. Mattos, G. Jacobs, B.H. Davis, F.B. Noronha, Production of hydrogen from ethanol: review of reaction mechanism and catalyst deactivation, *Chem. Rev.* 112 (2012) 4094–4123, <https://doi.org/10.1021/cr2000114>.
- [11] M. Ni, D.Y.C. Leung, M.K.H. Leung, A review on reforming bio-ethanol for hydrogen production, *Internat. J. Hyd. Energ.* 32 (2007) 3238–3247, <https://doi.org/10.1016/j.ijhydene.2007.04.038>.
- [12] C. Zhang, X. Qin, Z. Xue, X. Wang, Y. Shen, J. Zhu, Y. Wu, B. Meng, X. Meng, N. Yang, NaCl induced active hcp Co nanosheet for hydrogen production and formaldehyde abatement by formaldehyde steam reforming, *Chem. Eng. J.* 433 (2022), <https://doi.org/10.1016/j.cej.2022.134600>, 134600, 10.
- [13] R. Kriegel, D.C.A. Ivarsson, M. Armbrüster, Formic acid decomposition over ZnPd—implications for methanol steam reforming, *ChemCatChem* 10 (2018) 2664–2672, <https://doi.org/10.1002/cctc.201800194>.
- [14] C. Rameshan, C. Weilach, W. Stadlmayr, S. Penner, H. Lorenz, M. Hävecker, R. Blume, T. Rocha, D. Teschner, A. Knop-Gericke, R. Schlögl, D. Zemlyanov, N. Memmel, G. Rupprechter, B. Klötzer, Steam reforming of methanol on PdZn near-surface alloys on Pd(1 1 1) and Pd foil studied by in-situ XPS, LEIS and PM-IRAS, *J. Catal.* 276 (2010) 101–113, <https://doi.org/10.1016/j.jcat.2010.09.006>.
- [15] L. Barattini, G. Ramis, C. Resini, G. Busca, M. Sisani, U. Costantino, Reaction path of ethanol and acetic acid steam reforming over Ni–Zn–Al catalysts. Flow reactor studies, *Chem. Eng. J.* 153 (2009) 43–49, <https://doi.org/10.1016/j.cej.2009.06.002>.
- [16] S.M. de Lima, A.M. da Silva, L.O.O. da Costa, J.M. Assaf, G. Jacobs, B.H. Davis, L. V. Mattos, F.B. Noronha, Evaluation of the performance of Ni/La₂O₃ catalyst prepared from LaNiO₃ perovskite-type oxides for the production of hydrogen through steam reforming and oxidative steam reforming of ethanol, *Appl. Catal. A: General* 377 (2010) 181–190, <https://doi.org/10.1016/j.apcata.2010.01.036>.
- [17] Q. Jin, A. Wang, B. Lu, X. Xu, Y. Shen, Y. Zeng, Steam reforming of formaldehyde for generating hydrogen and coproducing carbon nanotubes for enhanced photosynthesis, *Catal. Sci. Technol.* 10 (2020) 4436–4447, <https://doi.org/10.1039/D0CY00843E>.
- [18] Q. Jin, Y. Shen, Y. Cai, L. Chua, Y. Zeng, Resource utilization of waste V₂O₅-based deNO_x catalysts for hydrogen production from formaldehyde and water via steam reforming, *J. Hazard. Mater.* 381 (2020), 120934, <https://doi.org/10.1016/j.jhazmat.2019.120934>.
- [19] H. Lorenz, M. Friedrich, M. Armbrüster, B. Klötzer, S. Penner, ZnO is a CO₂-selective steam reforming catalyst, *J. Catal.* 297 (2013) 151–154, <https://doi.org/10.1016/j.jcat.2012.10.003>.
- [20] T. Bielz, H. Lorenz, P. Amann, B. Klötzer, S. Penner, Water–gas shift and formaldehyde reforming activity determined by defect chemistry of polycrystalline In₂O₃, *J. Phys. Chem. C* 115 (2011) 6622–6628, <https://doi.org/10.1021/jp111739m>.
- [21] K. Ploner, M. Watschinger, P.D.K. Nezhad, T. Götsch, L. Schlicker, E.-M. Köck, A. Gurlo, A. Gili, A. Doran, L. Zhang, N. Köwitsch, M. Armbrüster, S. Vanicek, W. Wallisch, C. Thurner, B. Klötzer, S. Penner, Mechanistic insights into the catalytic methanol steam reforming performance of Cu/ZrO₂ catalysts by in situ and operando studies, *J. Catal.* 391 (2020) 497–512, <https://doi.org/10.1016/j.jcat.2020.09.018>.
- [22] M. Martinelli, N. Alhraki, J.D. Castro, M.E. Matamoros, G. Jacobs, in: S. Nanda, D.-V. Vo, P.N. Tri (Eds.), *Effect of Na Loading on Pt/ZrO₂ Catalysts for Low Temperature Water-Gas Shift for the Production and Purification of Hydrogen*, Chapter 6 in *New Dimensions in Production and Utilization of Hydrogen*, Elsevier Books, Amsterdam, The Netherlands, 2020, pp. 143–160 (ISBN: 9780128195536).
- [23] M. Martinelli, J.D. Castro, N. Alhraki, M.E. Matamoros, A.J. Kropf, D.C. Cronauer, G. Jacobs, Effect of sodium loading on Pt/ZrO₂ during ethanol steam reforming, *Appl. Catal. A: General* 610 (2021), 117947, <https://doi.org/10.1016/j.apcata.2020.117947>.
- [24] Z. Rajabi, M. Martinelli, C.D. Watson, D.C. Cronauer, A.J. Kropf, G. Jacobs, Lithium promotion of Pt/m-ZrO₂ catalysts for low temperature water-gas shift, *Internat. J. Hyd. Energ.* 47 (2022) 30872–30895, <https://doi.org/10.1016/j.ijhydene.2022.03.022>.
- [25] Z. Rajabi, M. Martinelli, G.F. Upton, C.D. Watson, D.C. Cronauer, A.J. Kropf, G. Jacobs, Low temperature ethanol steam reforming: selectivity control with lithium doping of Pt/m-ZrO₂, *Catal. Today* 402 (2022) 335–349, <https://doi.org/10.1016/j.cattod.2022.06.018>.
- [26] C.D. Watson, M. Martinelli, D.C. Cronauer, A.J. Kropf, C.L. Marshall, G. Jacobs, Low temperature water-gas shift: optimization of K loading on Pt/m-ZrO₂ for enhancing CO conversion, *Appl. Catal. A: General* 598 (2020), <https://doi.org/10.1016/j.apcata.2020.117572>, 117572, 17.
- [27] M. Martinelli, R. Garcia, C.D. Watson, D.C. Cronauer, A.J. Kropf, G. Jacobs, Promoting the selectivity of Pt/m-ZrO₂ ethanol steam reforming catalysts with K and Rb dopants, *Nanomaterials* 11 (2021) 2233, 24, <https://doi.org/10.3390/nano11092233>.
- [28] C.D. Watson, M. Martinelli, D.C. Cronauer, A.J. Kropf, G. Jacobs, Low temperature water-gas shift: enhancing stability through optimizing Rb loading on Pt/ZrO₂, *Catalysts* 11 (2021) 210, 30, <https://doi.org/10.3390/catal11020210>.
- [29] Z. Rajabi, M. Martinelli, C.D. Watson, D.C. Cronauer, A.J. Kropf, G. Jacobs, Influence of Cs loading on Pt/m-ZrO₂ water-gas shift catalysts, *Catalysts* 11 (2021) 570, 25, <https://doi.org/10.3390/catal11050570>.
- [30] Z. Rajabi, L. Jones, M. Martinelli, D. Qian, D.C. Cronauer, A.J. Kropf, C.D. Watson, G. Jacobs, Influence of Cs promoter on ethanol steam-reforming selectivity of Pt/m-ZrO₂ catalysts at low temperature, *Catalysts* 11 (2021) 1104, 22, <https://doi.org/10.3390/catal11091104>.
- [31] J.C. Lavalle, Infrared spectrometric studies of the surface basicity of metal oxides and zeolites using adsorbed probe molecules, *Catal. Today* 27 (1996) 377–401, [https://doi.org/10.1016/0920-5861\(95\)00161-1](https://doi.org/10.1016/0920-5861(95)00161-1).
- [32] G. Busca, V. Lorenzelli, Infrared spectroscopic identification of species arising from reactive adsorption of carbon oxides on metal oxide surfaces, *Mater. Chem.* 7 (1982) 89–126, [https://doi.org/10.1016/0390-6035\(82\)90059-1](https://doi.org/10.1016/0390-6035(82)90059-1).